University of Groningen

Surface roughness of gold substrates at the nanoscale

Solhjoo, Soheil; Vakis, Antonis I.

IMPORTANT NOTE: You are advised to consult the publisher's version (publisher's PDF) if you wish to cite from it. Please check the document version below.

Document Version
Final author's version (accepted by publisher, after peer review)

Publication date:
2017

[Link to publication in University of Groningen/UMCG research database](#)

Surface roughness of gold substrates at the nanoscale: an atomistic simulation study

Soheil Solhjoo, and Antonis I. Vakis*

Advanced Production Engineering, Engineering and Technology Institute Groningen, Faculty of Science and Engineering, University of Groningen, Nijenborgh 4, 9747 AG Groningen, the Netherlands

*Corresponding author: a.vakis@rug.nl; +31 50 363 4202

Abstract

The statistical properties of rough surfaces at the nanoscale are studied using classical molecular dynamics. Atomistic fcc blocks of gold are generated with different crystal orientations, and with rough surfaces having the same root-mean-square roughness with variable power spectral density (PSD) slopes and roll-off wavenumbers. The process of rough surface generation may result in thermodynamically unstable sharp spatial features. In order to relax the structure, the blocks are equilibrated at 300 K. It is found that all surfaces experience changes in their roughness, regardless of their crystal orientation or temperature, although the changes are only temperature-independent when $T \leq 0.4 T_\mathrm{m}$. Based on the analyzed PSDs of the equilibrated substrates, two methods for generating pseudo-stable rough surfaces are introduced and discussed.

Keywords: nanoscale, surface roughness, atomistic models, classical molecular dynamics.

1. Introduction

As a consequence of the miniaturization of mechanical devices, a large number of tribological research studies have been directed toward the atomic scale. Due to the limited lateral resolution of measuring devices in comparison to atomic spacing, researchers utilize atomistic computer simulation methods, e.g. classical molecular dynamics (MD), in order to investigate different tribological processes, such as normal or frictional contacts. In these works, the substrate is usually represented, either, as a flat or a simple patterned surface. One can also find a limited number of tribological MD studies which employed randomly rough substrates [1-12]; however, due to limitations in the lateral resolution of measuring devices, the nature of the atomic-scale roughness present on real surfaces is still under question. An important result stems from the work of Oliver et al. [13] who studied the morphology of tungsten nanoparticles using field-ion microscopy, and showed they have a stepped geometry; this was later used

1

for studying atomistic contacts [14], and also, for identifying the surface atoms via their potential energies [15]. On the other hand, the properties required to accurately generate a realistic rough surface at the atomic scale have yet to be investigated thoroughly.

In this paper, various randomly rough surfaces were generated and used for building atomic blocks of pure gold. Then, the blocks were equilibrated via classical MD simulations, and the effects of different parameters, such as temperature and crystal orientation, on the equilibrated blocks were studied. The results show that the atomistic substrates cannot retain their sharp steps and edges, and the surfaces are smoothened due to thermodynamic considerations. This has important consequences in the performance of atomistic simulations, where emphasis should be placed on using physically meaningful surface topographies.

2. Quasi self-affine rough surfaces

The random nature of surface roughness, which is always present at some length scale, can be described statistically. One of the most widely used descriptions of random surfaces was introduced by Nayak [16]; through the translation of rough surfaces from the Cartesian space into the Fourier one, Nayak represented the height function $h(\mathbf{p})$ (where $\mathbf{p} = (x, y)$ is a 2D vector in the plane $z = 0$) of homogeneous-isotropic-Gaussian surfaces as

$$h(\mathbf{p}) = \sum_{\mathbf{q}} h(\mathbf{q}) \cos(\mathbf{q} \cdot \mathbf{p} + \varphi(\mathbf{q})).$$

Eq. 1

where $\mathbf{q}$ is the wavevector with q_x and q_y as its components, $h(\mathbf{q})$ is the height roughness spectrum and contains the coefficients of the discrete Fourier transform of the rough surface, and $\varphi(\mathbf{q})$ is a phase shift, randomly and uniformly distributed over $[0, 2\pi)$. In order to generate real numbers for $h(\mathbf{p})$ using Eq. 1, the values of $h(\mathbf{q})$ and $\varphi(\mathbf{q})$ should be defined in a way that $h(-\mathbf{q}) = h(\mathbf{q})$ and $\varphi(-\mathbf{q}) = -\varphi(\mathbf{q})$. The coefficients $h(\mathbf{q})$ are related to the power spectral density (PSD) of the surface, $C(\mathbf{q})$, which is the Fourier transform of the autocorrelation function of the surface, via $h(\mathbf{q}) = (2\pi/L)|C(\boldsymbol{q})|^{1/2}$ [17], where L is the length of the system.

2.1. The PSD of isotropic self-affine surfaces

For the case of isotropy of the surface, $C(\mathbf{q})$ can be averaged to construct $C(q)$, where q is the

wavenumber that corresponds to the magnitude of the wavevector $\mathbf{q}$, i.e. $q = \|\mathbf{q}\|$. One of the models for describing the PSD of a self-affine surface, which has been widely used in the field of contact mechanics, has a simple formulation in the form Eq. 2:

$$C(\mathbf{q}) = \begin{cases} C_0 & q_L \leq \|\mathbf{q}\| < q_r \\ C_0(\|\mathbf{q}\|/q_r)^\beta & q_r \leq \|\mathbf{q}\| \leq q_S, \\ 0 & \text{elsewhere} \end{cases} \qquad \text{Eq. 2}$$

where β is referred to as "the PSD exponent" in this text and has a negative value, and C_0 is a constant. Appendix A and Appendix B provide detailed discussions on the values of β and C_0. The range of wavenumbers is bounded by the long and short wavelength cutoffs denoted by q_L and q_S, respectively. The lowest possible wavenumber is connected to the length of the system, L, and its value is $q_L = 2\pi/L$, while the highest possible wavenumber is related to the shortest wavelength, i.e. the shortest distance between two sampled neighboring points, δ, and its value is $q_S = 2\pi/\delta$. From this definition, it follows that q_S depends on the lateral resolution of measuring instruments. Moreover, q_r is the roll-off wave number, with $q_L < q_r < q_S$. Figure 1 shows a schematic PSD corresponding to the definition of Eq. 2.
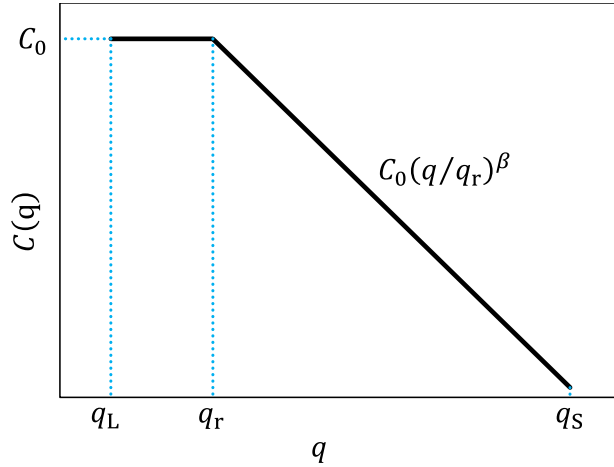
Figure 1. The schematic power spectral density, plotted in a full logarithmic scale, based on the definition of Eq. 2.

The definition of the PSD in the form of Eq. 2 is based on the Bhushan and Majumdar discovery of bifractal surfaces through analyzing magnetic tapes using atomic force microscopy [18]. The characterization of bifractal surfaces was discussed by Wu [19]: a bifractal surface has a critical wavenumber q_c in its PSD such that the PSD exponent is different for wavenumbers larger and smaller

3

than q_c. If $q_r \neq q_L$, Eq. 2 results in a bifractal surface with $q_c = q_r$. The definition of bifractal surfaces can be more complicated, e.g. see [20, 21]. While most models have different formulae for wavenumbers larger or smaller than q_c, the PSD of isotropic self-affine surfaces can be defined based on the K-correlation function, developed by Palasantzas [22], in the following form [23]:

$$C(q) = \frac{(\zeta \sigma_{\mathrm{rms}})^2}{2\pi} \left(1 - \frac{\zeta^2}{\beta + 2} q^2 \right)^{\beta/2}, \qquad \text{Eq. 3}$$

where ζ is the lateral correlation length, which is defined using the autocorrelation function $R(r)$ of the surface: more specifically, ζ is the value of r at which $R(r = \zeta) = \exp(-1)$ [23]. It should be noted that $\beta < -2$ in this model. Although this model can describe the behavior of bifractal surfaces, it does not require any critical wavenumber.

3. Atomic blocks with rough surfaces and the necessity of equilibration

In order to generate an atomic block with a rough surface, the first step is to generate the rough surface as a point cloud of spatial coordinates, which will then be used for cutting an atomic block [2]. In the process of cutting, one may include the data points of the rough surface to preserve its spatial features [2] (see Figure 2); however, this would result in an unrealistic structure, with atoms being stacked closer together than possible in a real system. Depending on the resolution of the generated surface, this method can remove any sharp atomic steps and provide a smoother surface. In contact mechanics studies, this feature yields results closer to those of continuum mechanics theories, e.g. see [24]; however, because of the artificially high atomic density at the surface, the applicability of this method is limited to non-adhesive contacts, where only repulsion is accounted for, and cannot be used for studying adhesive contacts. Moreover, the lack of knowledge on the nature of roughness at the atomic scale limits researchers to data measured at larger scales: the vertical resolution along the height dimension can be down to the atomic level, but the lateral resolution of most instruments is still of the order of tens of nanometers. It should be mentioned that, if an atomic block is generated by this method, the block should be treated as a completely rigid material, otherwise the high surface density will result in instability of the system. On the other hand, it is possible to cut the atomic block without imposing the rough surface data points to the system, resulting in an atomic block that would not have an artificially high atomic density; however, in this latter case, which is the focus of the present work, atomic steps and edges are unavoidable.

4

The sections of two representative atomic blocks with rough surfaces are depicted in Figure 2: the prevalence of atomic steps is clearly shown. In the figure, the two rough surfaces were compared through their lateral correlation lengths, ζ: a larger value of ζ corresponds to smoother features.
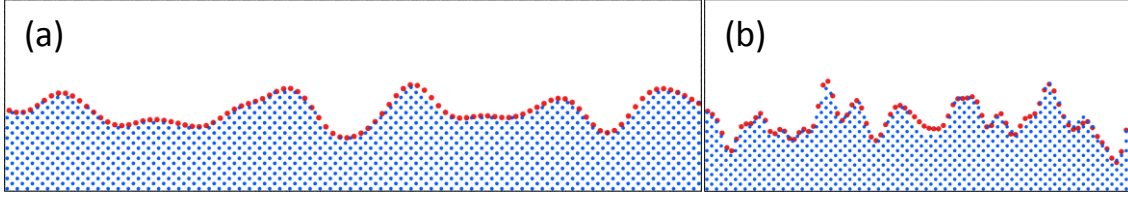

Figure 2. Slices of two atomistic blocks generated by different arbitrary rough surfaces with lateral correlation lengths of (a) $\sim$21 Å and (b) $\sim$7 Å. The smaller/blue dots indicate the atoms positioned based on their crystal structure descriptions, and the larger/red dots indicate the data points of the surface imposed to the system as additional atoms.

When investigating rough surface contact with classical molecular dynamics, the atomic block needs to be relaxed from all arbitrarily assigned initial conditions so that the system can approach an equilibrated new state point [25, 26]. In this study, atomic blocks were sliced with different numerical rough surfaces (without imposing the numerical rough surface as additional atoms; see discussion in earlier paragraph) and the resulting rough atomic blocks were analyzed by examining their statistical properties.

4. Simulation procedure

4.1. Generating the rough substrates based on the simplified PSD

The randomly rough surface generation was performed with the algorithm described by Persson et al. [17] and Rigazzi [27], by specifying the lattice constant $\delta = a_0$, where a_0 is the lattice parameter of the simulated material. The surfaces were generated with a lateral length L of $60a_0$. The highest wavenumber was set to $q_S = \pi/a_0$. The roughness of the generated surfaces was varied by changing the values of the roll-off wavenumber and the PSD exponent: the roll-off wavenumber was defined as $q_r(i) = q_L^{1-i/4} q_S^{i/4} = q_L(L/\delta)^{i/4}$ with $i \in \{1, 2, 3\}$, and different values for the PSD exponent were selected where $\beta \in [-1, -5]$. The corresponding values of C_0 were defined based on Eq. B3, in order to set the RMS roughness at $2a_0$ (see Appendix B). It should be noted that $\beta = -2$ resulted in an undefined value of I_0 (see Eq. B4) for which the surfaces cannot be generated; therefore, β was approximated by setting its value to -2.001.

Table 1 summarizes all the simulated rough surfaces: the surfaces are designated via their roll-off wavenumber and PSD exponent values, e.g. $q1$ denotes surfaces with $q_r(i = 1)$, and $\beta 3$ refers to surfaces whose initial PSD exponent was -3; along these lines, $q1\_\beta 3$ points to the surface with $q_r(i = 1)$ and $\beta = -3$.

Table 1. All the surfaces generated based on the PSD of Eq. 2. The q_r values, normalized by q_L, for $i = 1$, 2, and 3 would be 2.78, 7.75, and 21.56, respectively.

	$\beta = -1$	$\beta \cong -2$	$\beta = -3$	$\beta = -4$	$\beta = -5$
$q_r(i = 1)$	$q1\_\beta 1$	$q1\_\beta 2$	$q1\_\beta 3$	$q1\_\beta 4$	$q1\_\beta 5$
$q_r(i = 2)$	$q2\_\beta 1$	$q2\_\beta 2$	$q2\_\beta 3$	$q2\_\beta 4$	$q2\_\beta 5$
$q_r(i = 3)$	$q3\_\beta 1$	$q3\_\beta 2$	$q3\_\beta 3$	$q3\_\beta 4$	$q3\_\beta 5$

Each of the generated rough surfaces was used for constructing a rough atomic block. To do so, a thick block of gold with a lattice parameter of $a_0 = 4.078$ Å [28] was constructed. Then, the cutting procedure was applied by placing the rough surface at a position where the distance from the bottom of the block and the minimum height of the surface was $10a_0$; in other words, each block had a minimum thickness of $10a_0$.

4.2. The equilibration procedure

A number of substrates with specific rough surfaces were generated by means of the PSD in the form of Eq. 2, as described in section 4.1. In order to resolve the unstable atomic steps of the generated rough substrates, these needed to be equilibrated. This procedure was performed with classical molecular dynamics via the large-scale atomic/molecular massively parallel simulator (LAMMPS) [29]. The equations of motion were solved using the velocity-Verlet algorithm [30] with a step size of 10 fs [31]. This time step was tested by a pre-test simulation of NVE-ensemble to make sure that the system does not exhibit any energy drift. Periodic boundary conditions (PBCs) were applied along the lateral directions. Also, the atoms of the lowest layer were not allowed to move in the z direction. The embedded atom method (EAM) potential [32], with the database developed by Sheng et al. [28], was used for governing the atoms. The temperature was set at 300 K by applying Berendsen's thermostat [33] to all atoms, and the damping constant was set to 0.1 ps. The equilibration procedure was performed for 1.5 ns.

The effects of roughness, crystal orientation, and temperature were investigated in this work. The details

of the roughness parameters are described in section 4.1. In order to study the effects of the crystal orientation, different atomic blocks were used in the cutting process; the blocks were dissimilar regarding their crystalline directions along the z coordinate direction. Three dissimilar blocks with crystalline directions of $[100]$, $[110]$, and $[111]$ along the z axis were used in this study. It should be noted that the effects of crystal orientation were studied only on a number of selected systems (see section 5.4 for the details), and for the other systems, the $[100]$ direction was set along the z axis. Moreover, the effects of temperature were studied for one selected system (see section 5.5 for the details). The temperature was set at different values between zero Kelvin and the melting point of $T_{\mathrm{m}} = 1281\ \mathrm{K}$ [28]. It should be noted that the relaxation at zero Kelvin was done by the molecular statics method, using the Polak-Ribiere version of the conjugate gradient algorithm [34]. This minimization technique iteratively adjusts atoms coordinates in a direction with the steepest potential energy gradient. The procedure continues until the system reaches its local potential energy minimum.

4.3. Roughness analyses of the equilibrated substrates

In order to analyze the roughness of the equilibrated substrates, it was first necessary to identify surface atoms. To do so, the method described in Ref. [15] was utilized: a spherical gold particle with a radius of $50\ \text{Å}$ and a stepped geometry was equilibrated at $300\ \mathrm{K}$, and the values of the potential energy were used as a criterion for identifying surface atoms, as shown in section 5.1. The visualization and structural analyses of the systems were performed using OVITO [35].

Once the surface atoms were identified, their spatial coordinates were used for fitting a surface of the form $h(\mathbf{p})$ to them, using a triangulation-based linear interpolation function, e.g. see [36]. For the fitting process, the $\mathbf{p}$-space extended over $[0,0]$ and $[L, L]$ with a grid spacing of δ = a0. Considering $L = 60a_0$, a 60×60 grid was used for a $\mathbf{p}$-space of size $L \times L$. Then, the fitted surfaces were analyzed for their relevant roughness parameters.

It should be noted that the atoms' positions were not saved as an averaged value over a period of time; the surface analysis was done for each system over the equilibration times between 1.1 ns and 1.5 ns (see Figure 4); i.e. each system was analyzed at the different time steps in which the equilibration was achieved, and the average values were reported.
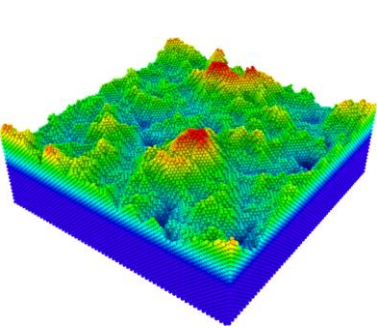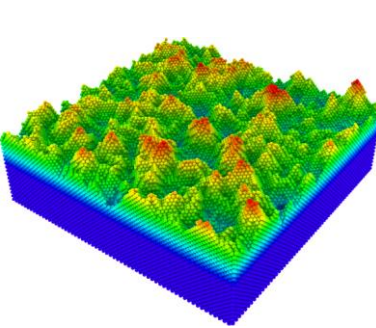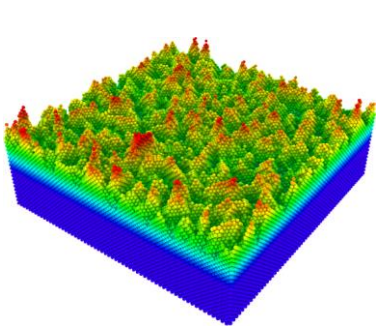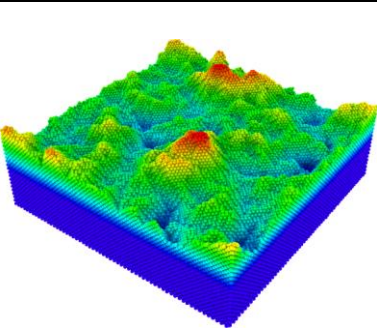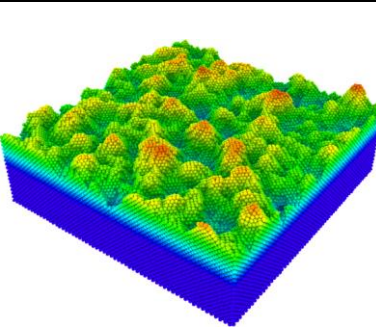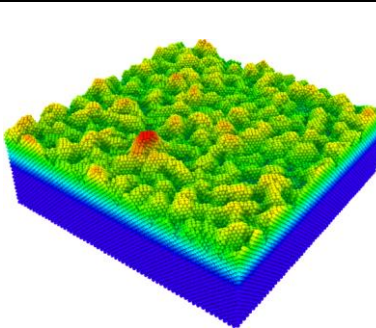
5. Results and discussion

Table 2 illustrates the rough surfaces of the $\beta 3$ systems, equilibrated at $300\ \mathrm{K}$. The $q3\_\beta 3$ system

changed in a way that removed a number of sharp atomistic edges, as can be seen by the significant reduction of sharp peaks and their coalescence into smoother ones in the equilibrated surface. The changes in $q2\_\beta3$ are smaller, and the changes in $q1\_\beta3$ can barely be noticed. It should be noted that, although the global minimum potential of the systems would be reached when the substrates are flat, the equilibration process led the systems to their local potential minimum. In other words, the roughness would not disappear unless an activation energy, for example, in the form of heat, is applied to the system to surpass the energy barrier between the local and global potential minima. The effects of temperature were investigated, and the results are discussed in section 5.5.

Table 2. The atomistic $\beta3$ rough substrates with the $[100]$ crystalline direction along their z axis before and after equilibration process. The atoms are colored based on their height values, ranging between $\sim10a_0$ (blue) and $\sim22a_0$ (red).

5.1. Identifying the surface atoms at 300 K

In order to compare the rough surfaces in a quantitative way, first, the surface atoms were identified. This was done by defining a potential cutoff using a calibration test [15], which is based on the analyzing

the energy distribution of the surface atoms of a spherical nanoparticle. It should be noted that, although the total potential energy of the nanoparticle is not directly comparable with the potential energy of the bulk, due to its large surface area, the potential energy values of the nanoparticle's surface atoms are comparable with those of the surface atoms of the same material, regardless of its shape; therefore, the potential energy distribution of the nanoparticle's surface atoms can be used for identifying the surface atoms of the rough substrates. Figure 3 shows the outer shell of the equilibrated particle, and the potential energy distribution of its atoms. The minimum energy between the δ and ι peaks was selected as the potential cutoff, and its value was found to be $PE_c = -3.5380 \pm 0.0004$ eV. It should be noted that this characteristic potential energy was found to be independent from the applied temperature. Identifying the surface atoms using their potential energy values is very fast, because a simple comparison between the saved potential energies and the cutoff can be used for this identification, and no extra computation is required. Its applicability, however, is limited to perfect crystals, and, if the system has some defects or is not crystalline, other post-processing methods should be applied. For example, the system can be analyzed via a gridding algorithm; see section 5.5 for a discussion on this method.
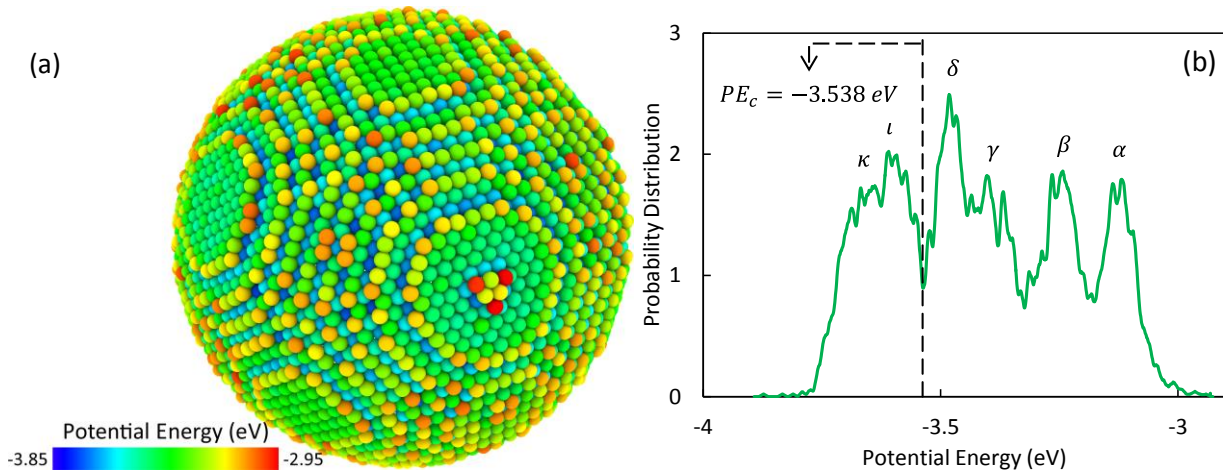
Figure 3. (a) A gold spherical particle with a stepped geometry, equilibrated at 300 K. The atoms are colored using their potential energy values. (b) The potential energy distribution of the shell atoms of the equilibrated gold particle. The vertical line indicates the value that divides the partially contacting atoms from the rest, i.e. PE_c.

The main reason for the configuration changes was the reduction in the potential energy of the surface atoms. Sharp atomic steps and edges impose a high energy value; hence, thermodynamically, the potential energy is reduced until a more stable level is achieved with the removal of high frequency

spatial features. The changes in the potential energy were studied by extracting the potential energies of the surface atoms, i.e. atoms with a potential energy higher than the cutoff $PE_c = -3.538$ eV. Then, the average values per atom were calculated, as is shown in Figure 4. As the results show, the potential energy of the surface atoms dropped rapidly during the equilibration; however, after the first drop, the changes became smaller in magnitude. Moreover, the results show that the selected relaxation time of 1.5 ns was long enough for the potential energies of all systems to reach a steady state.
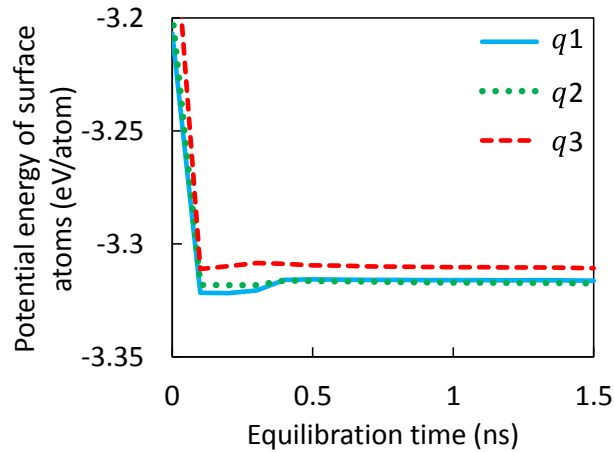
Figure 4. The average potential energy per atom (eV/atom) of the surface atoms of the studied systems during the equilibration process, at 300 K.

By applying the potential cutoff $PE_c = -3.538$ eV, the surface atoms were identified. After the identification of the surface atoms, these were fitted by a surface. Figure 5 illustrates the identified surface atoms and the fitted surface of the equilibrated $q1\_\beta3$ system. The fitted surfaces were used for surface analysis; the results are presented and discussed in the following sections.

10

Figure 5. This figure illustrates (left) the identified surface atoms, and (right) the fitted surface of the $q1\_\beta3$ system. The identified surface atoms were used for fitting a roug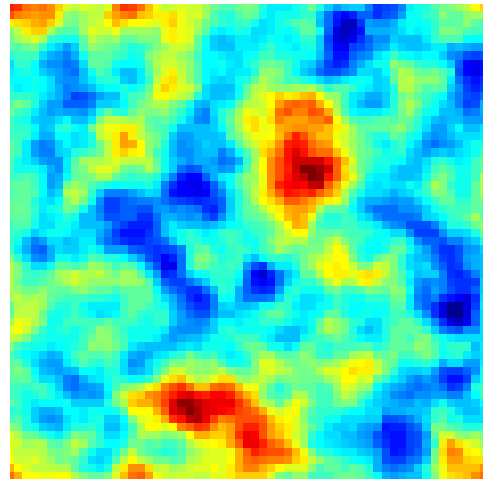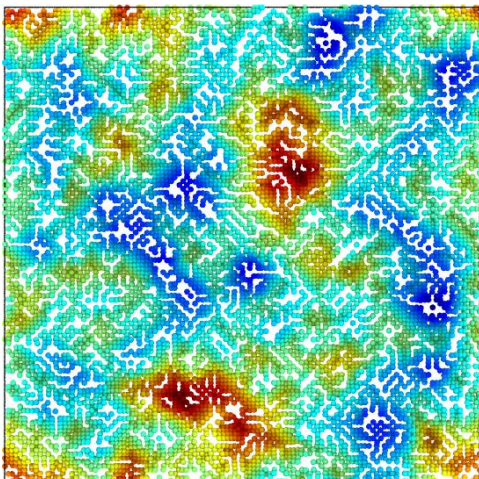h surface using a 60×60 uniform grid. This procedure was followed for all of the systems, and the surface analyses were done on the fitted surfaces. In this figure, the atoms and grids are colored based on their height values: valleys and peaks are colored as blue and red, respectively.

5.2. Roughness for $z = [100]$ at 300 K

Three sets of substrates, $q1$, $q2$, and $q3$, with crystal direction $[100]$ along their z axis were equilibrated at 300 K. The roughness of the substrates was characterized via three statistical parameters: lateral correlation length ζ (see section 3), RMS gradient $\overline{g} = \sqrt{\langle |\nabla h(\mathbf{p})|^2 \rangle}$, and RMS roughness $\sigma_{\mathrm{rms}} = \sqrt{\langle |h(\mathbf{p})|^2 \rangle}$. Figure 6 shows the lateral correlation length and RMS gradient for the rough surfaces, both, before and after equilibration. For the generated surfaces, the lowest lateral correlation length and the highest RMS gradients were calculated to be $\zeta_{\mathrm{min}} \cong 0.5a_0$ and $\overline{g}_{\mathrm{max}} = 2.08$, respectively. While these two values were not controlled in the surface generating process, some limiting values were found for these two parameters in the equilibrated state: $\zeta_{\mathrm{min}} \cong \sqrt{2}a_0$ and $\overline{g}_{\mathrm{max}} \cong 1$. While the maximum value of $\overline{g}_{\mathrm{max}} \cong 1$ was smaller than the maximum limiting value of $\sqrt{2}$ for nominally flat rough atomistic surfaces (see Appendix C), $\zeta_{\mathrm{min}} \cong \sqrt{2}a_0$ can be related to the shortest possible wavelength $\lambda_{\mathrm{min}} = 2\sqrt{2}a_0$ in an fcc structure, which is four times the shortest interatomic distance in that crystalline structure. Moreover, Figure 6 shows that σ_{rms} for all generated surfaces was originally close to the assigned value of $\sigma_{\mathrm{rms}} = 2a_0$. The values of σ_{rms} of the equilibrated systems, however, changed to lower values with different magnitudes.
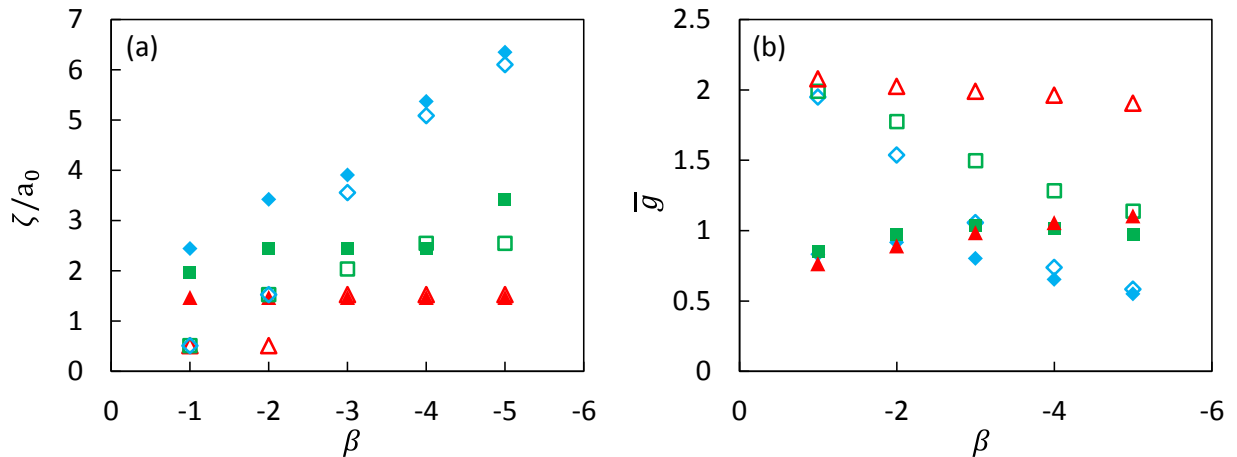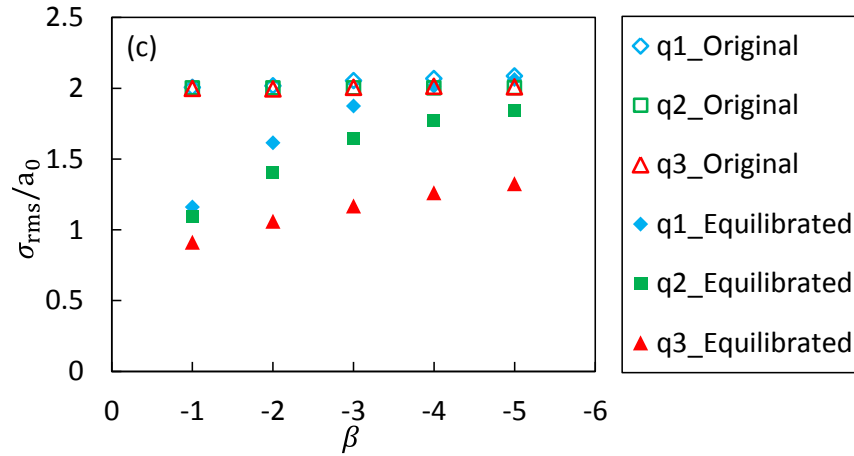
Figure 6. The statistical parameters of the rough surfaces: (a) the lateral correlation length normalized by the lattice constant, (b) the RMS gradient, and (c) the RMS roughness normalized by the lattice constant. Note that the systems are differentiated using their q_r values, as described in section 4.1.

Before further investigation, let us define a hybrid roughness parameter $\rho = \sigma_{rms}\overline{g}/\zeta$: for a flat surface ($\sigma_{rms} = 0$, $\overline{g} = 0$ and $\zeta = \infty$) $\rho = 0$, and ρ increases as the surface becomes rough with random roughness features, which results in higher values of σ_{rms} and $\overline{g}$ and lower values of ζ. Figure 7 (a) shows how the roll-off wavenumber and PSD exponent affect the roughness of the original substrates: higher assigned values of q_r and β resulted in rougher surfaces. In order to compare the roughness parameters before and after the equilibration, their relative change was calculated via $|\Delta\rho|/\rho_0$ with $\Delta\rho = \rho_{EQ} - \rho_0$ where ρ_{EQ} and ρ_0 are the roughness of the equilibrated and original surfaces, respectively. The results are shown in Figure 8. This comparison shows that rougher surfaces experienced larger relative changes in their roughness.
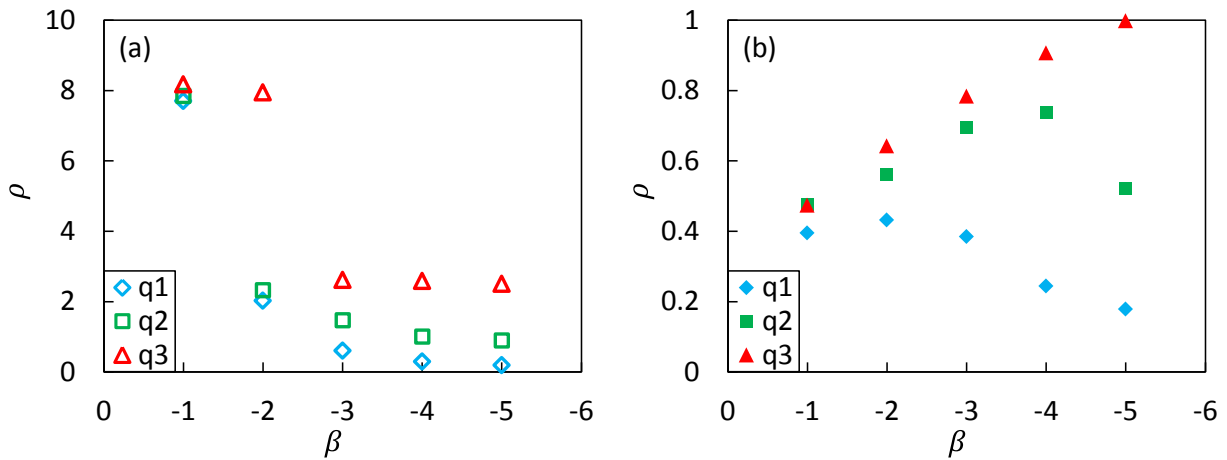
Figure 7. The roughness parameter ρ of the substrates (a) before, and (b) after the equilibration. Note

that the ranges of ρ differ by one order of magnitude between (a) and (b).
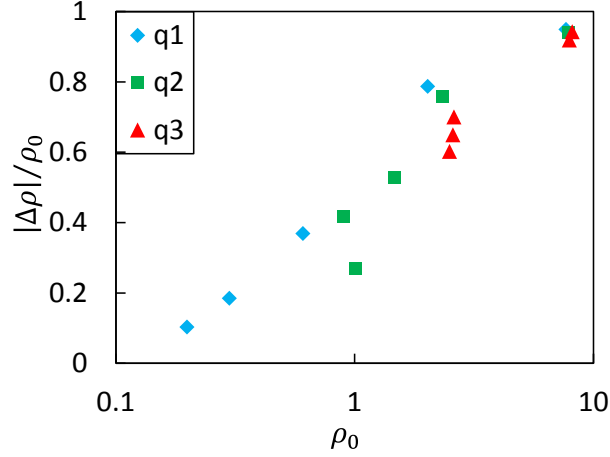
Figure 8. The changes of ρ as a function of the roughness of the original surfaces ρ_0.

Comparing the values of ζ and $\overline{g}$ with the corresponding values of ρ (see Figure S2), it was found that $\zeta_{\min} \cong \sqrt{2}a_0$ and $\overline{g}_{\max} \cong 1$ correspond to the roughest substrates, and as the substrates become smoother, i.e. $\rho \to 0$, the values of ζ and $\overline{g}$ increase and decrease, respectively. Moreover, the results show that the changes on the RMS roughness was more pronounced on rougher surfaces (see Figure S3). This is due to the fact that the "priority" for a rough surface during equilibration is to lower its energy by becoming smoother, and not to preserve any of its original statistical roughness parameters.

Furthermore, the values of skewness $S_{\mathrm{sk}} = \langle \hat{h}^3 \rangle / \langle \hat{h}^2 \rangle^{3/2}$ and kurtosis $S_{\mathrm{ku}} = \langle \hat{h}^4 \rangle / \langle \hat{h}^2 \rangle^2$, with $\hat{h} = h(\mathbf{p}) - \langle h(\mathbf{p}) \rangle$, and their changes due to equilibration process were calculated. Figure 9 shows that the skewness values of the height distribution for the original surfaces were close to zero for most systems. For almost all substrates, the equilibration process results in negative values of skewness, which indicates that the effect of the removal of sharp peaks was more dominant than that of the removal of deep valleys [37]. The kurtosis of most of the original rough surfaces was close to, or lower than 3, and the equilibration process lowered the value of this parameter, indicating that the surfaces had relatively few high peaks and low valleys [37]; however, the changes of kurtosis showed no discernible correlation (see Figure S4).
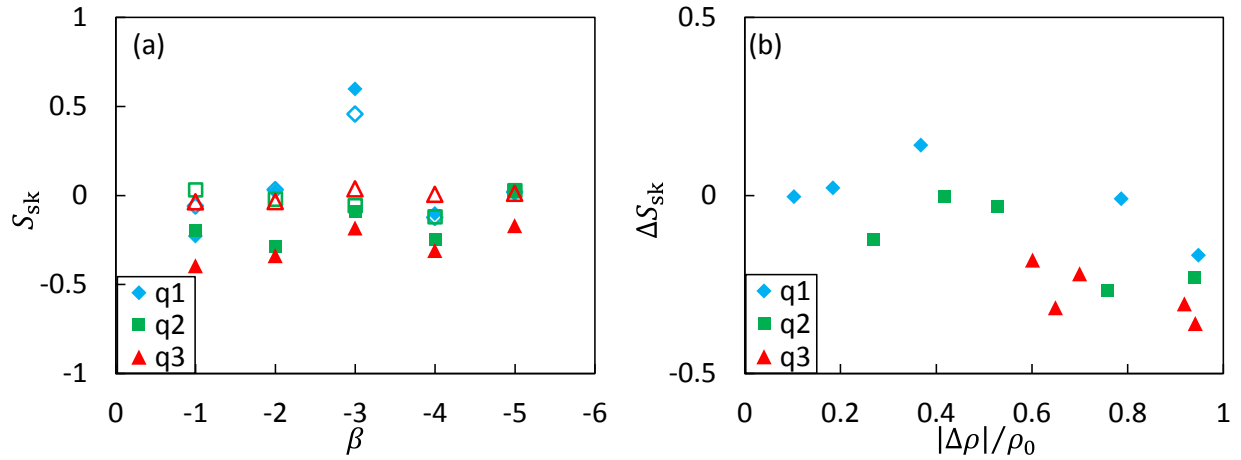
Figure 9. (a) The values of skewness of the original (void symbols) and equilibrated (filled symbols) surface roughness. (b) The changes of kurtosis due to the equilibration process.

The rough surfaces were investigated in more detail by analyzing their PSDs. Because the roughness of the substrates was periodic in the lateral directions, there was no need to average the roughness around the edges. Moreover, the highest frequency cutoff was defined using the shortest possible wavelength in the fcc structure, i.e. $q_S = 2\pi/\lambda_{min}$. Figure 10 shows the PSD of a number of selected systems. As the results show, the equilibrated surfaces lost their high frequency content, i.e. the sharp steps and edges; however, this deviation is not spread over the whole range of wavenumbers, but starts at a specific wavenumber designated as q_{dev} in the remainder of this paper: the equilibrated surfaces preserved their PSD values for wavenumbers smaller than q_{dev}. *The presence of q_{dev} for all of the substrates is evidence that surface roughness at the atomic scale has fractal characteristics with three segments.*
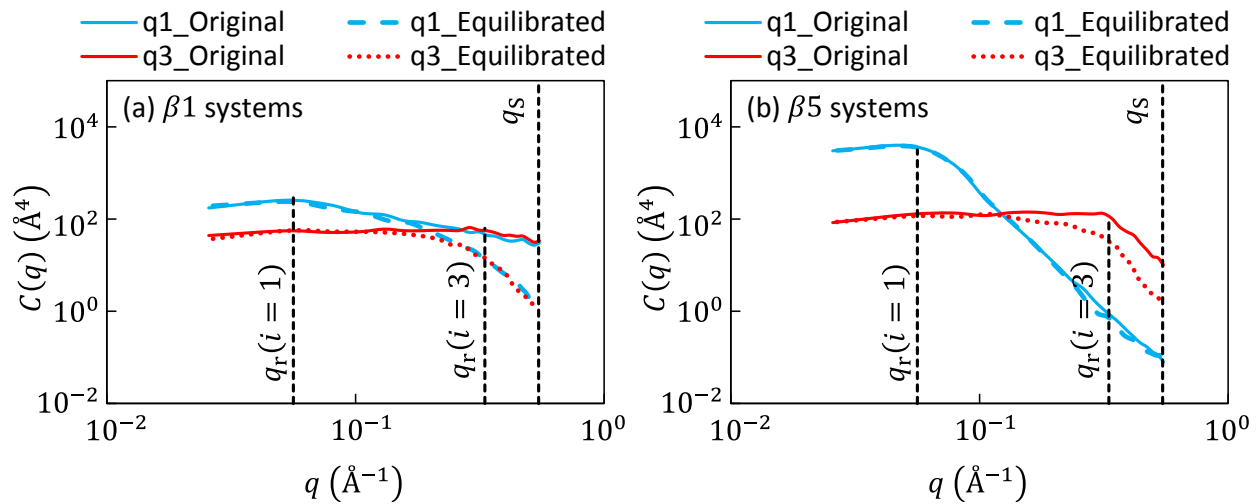
Figure 10. The PSDs of a number of selected systems of (a) $\beta = -1$, and (b) $\beta = -5$. Note that the $q2$

14

systems are not included in the figure for purposes of clarity. The small dashed lines show different parameters: q_S with a value of $\pi/\sqrt{2}a_0$ indicates the validity limit of the PSDs, $q_r(i)$ points to the roll-off wavenumber of the original PSDs, and q_{dev} in (a) shows the wavenumber at which the PSDs of the equilibrated surfaces deviate from the original PSDs.

In order to investigate this deviation, q_{dev} was defined as the smallest wavenumber at which $\left|\frac{C_{relaxed}-C_{original}}{C_{original}}\right| = 0.5$. Figure 11 shows the estimated values of q_{dev}. The results show that q_{dev} increases as the surface becomes smoother, which means that a smoother surface loses its original roughness features at higher frequencies compared to a rougher surface. Moreover, comparing the q_{dev} with the corresponding q_r shows whether the PSD has lost its original roll-off wavenumber or not: for $q_{dev} > q_r$ the roll-off wavenumber of the PSD would not change due to equilibration. Based on the results, it can be concluded that assigning lower values of q_r decreases q_{dev}, which means that the equilibration process does not affect the surface for a wider range of wavenumbers. Moreover, the $q3$ systems showed the smallest values of q_{dev} equal to ~ 1.585 Å^{-1}.
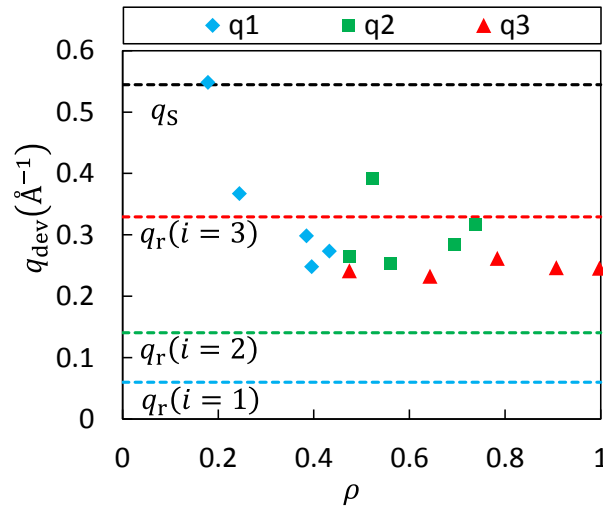
Figure 11. The estimated values of q_{dev} as a function of roughness parameter ρ. The q_r values are also shown for comparison.

Although q_{dev} points to the deviations of the PSD before and after equilibration, it is important to realize that the original PSD has a great impact even on the deviated section. This influence is illustrated in Figure 12, which compares the PSDs of two of the roughest substrates, i.e. $q3\_\beta1$ ($\rho = 0.87$) and $q3\_\beta5$ ($\rho = 0.61$). This comparison reveals that these two surfaces had very similar high frequency features; however, it is easily noticeable how the original $q_r(i = 3)$ affected the shape of the PSD for

15

wavenumbers between $q_r(i = 3)$ and the corresponding q_{dev}.
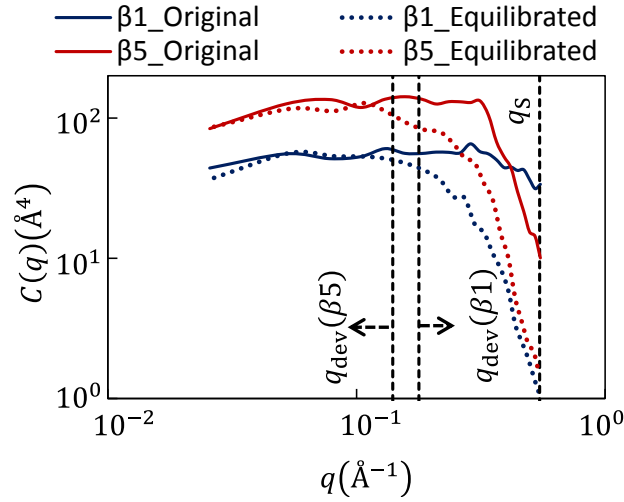
Figure 12. The PSDs of the $q3\_\beta1$ and $q3\_\beta5$ systems. Note that the results are copied from Figure 10.

Assuming a constant PSD exponent for the high frequencies of the surface roughness, the value of β was estimated. In this estimation, the wavenumbers were bounded between $q_S = \pi/\sqrt{2}a_0$ and the corresponding q_{dev}. It should be noted that this estimation was done only for the systems for which $q_{dev} \geq q_r$, i.e. systems $q1$ and $q2$. The results (summarized in Figure S5) suggest a trend of decreasing β for increasing roughness ρ.

5.3. Crystal defects due to equilibration process

While the focus of this work is to study surface roughness and its changes due to the equilibration process, the substrates were also analyzed to investigate whether the changes resulted in the generation and emission of dislocations. The analyses of all systems revealed that a few dislocation lines were generated only in the $q1\_\beta3$ system with a total length of $10\,nm$ (see Figure 13). Moreover, the generated dislocations did not grow, and stayed attached to the rough surface, signifying that much thinner substrates can be used for purposes of equilibration. Furthermore, the stress analysis showed that the equilibrated blocks were free of any locally accumulated stress. A detailed discussion can be found in the supplementary information.
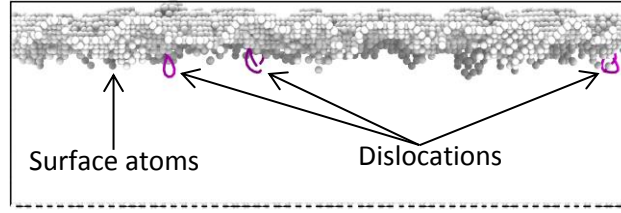
Figure 13. The surface atoms and the generated dislocation lines of the equilibrated $q1\_\beta3$ system. The outlines indicate the size of the simulation box.

5.4. Effects of crystal orientation

The effects of crystal orientation were studied for four limiting systems, namely $q1\_\beta1$, $q3\_\beta1$, $q1\_\beta5$, and $q3\_\beta5$, corresponding to the minimum and maximum values of q_r and β investigated. The results were the same as the ones reported in Figure 8, and the crystal orientation had negligible effects on the relative changes of roughness (see Figure S6). Moreover, the minimum lateral correlation length was found to be $\zeta_{min} \cong \sqrt{2}a_0$ and independent from the crystallographic orientation.

While the values of the RMS roughness, RMS gradient, and lateral correlation length were found to be independent from the crystallographic orientations, the skewness and kurtosis of the rough surfaces with higher values of β, i.e. those of the $\beta1$ system, showed dependency on the crystallographic orientations (see Figure S7). The results showed the smallest ranges of ΔS_{sk} and ΔS_{ku} for the systems with directions of $[110]$ and $[111]$ along their z axis, respectively; however, the $q1\_\beta5$ system showed the minimum changes of $\Delta S_{sk} = 0.04$ and $\Delta S_{ku} = 0.12$.

Moreover, the PSD of the rough surfaces were analyzed, and the values of q_{dev} were estimated (summarized in Figure S8). The results show that, for almost all systems, changing the crystal orientation from $[100]$ to, either, $[110]$ or $[111]$ resulted in larger values of q_{dev}; however, the value of q_{dev} for the $q3$ systems was smaller than $q_r(i = 3)$ for all directions, meaning that the equilibrated surfaces had lost their originally assigned roll-off wavenumber, regardless of the crystal orientation along the z axis.

5.5. Effects of temperature

In order to investigate the sensitivity of the results to temperature, the most stable system, $q1\_\beta5$, was selected and equilibrated at different temperatures ranging between absolute zero and the melting point of the simulated material, which is reported to be $T_m = 1281$ K [28]. Figure 14 shows the potential energy of the equilibrated systems as a function of temperature. In order to visibly show the melting

17

point, the heat capacity was estimated as $\Delta E / \Delta T$, where ΔE and ΔT are the changes in the potential energy and temperature between two data points. The sudden jump in the heat capacity between $T/T_{\mathrm{m}} = 0.8$ and $T/T_{\mathrm{m}} = 1.0$ indicates the melting of the system [31].
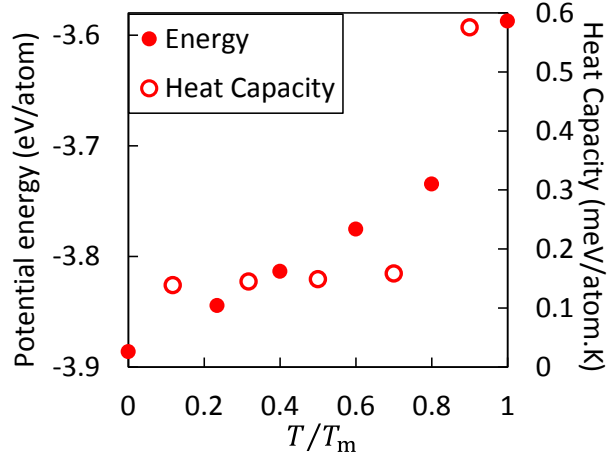
Figure 14. The equilibrated potential energy and heat capacity of the systems as a function of temperature.

For the systems at temperatures lower than $T/T_{\mathrm{m}} = 0.8$, the surface atoms were identified as described in section 5.1. For the molten system, however, this method would not work because the molten structure affects the potential energy and its distribution throughout the system. Therefore, the surface atoms were detected via a gridding algorithm: the system was divided by a bin size of a_0 along the x and y directions, and within each bin, the atom with the maximum z value was selected as the surface atom. The lateral correlation length and PSD of each rough surface was calculated, and the values of ρ and q_{dev} were estimated, as shown in Figure 15.
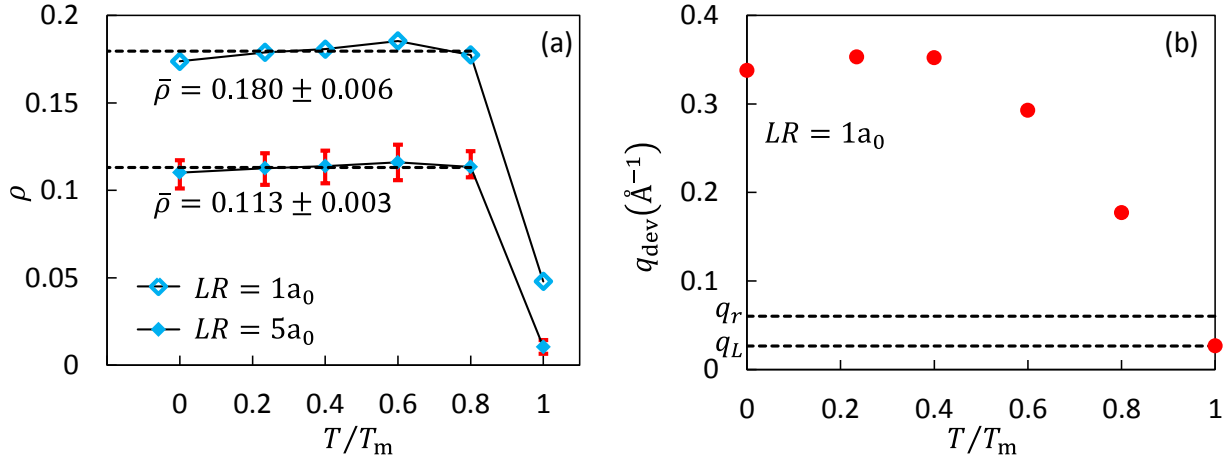
Figure 15. (a) Roughness as a function of equilibrating temperature and lateral resolution (LR). (b) The dependence of deviation wavenumber on equilibrating temperature. The average roughness $\bar{\rho}$ of each set was calculated based on the ρ values for $0 \leq T/T_m \leq 0.8$.

Figure 15 (a) shows the calculated roughness of the surface analyzed with two different lateral resolutions (LR) of $1a_0$ and $5a_0$. The lateral resolution indicates the lateral distance between two adjacent sampled data; $LR = 1a_0$ was selected to be consistent with the grid spacing used in the rough surface generating algorithm (see section 4.1), and $LR = 5a_0 \cong 2$ nm was selected to be comparable with the lateral resolution of measuring devices [38]. The results with $LR = 1a_0$ show that the roughness slightly increases by changing the equilibrating temperature from 0 K to $0.6T_m$, followed by a slight decrease for $T/T_m = 0.8$, and a sudden drop at the melting point. The mean roughness value of the surface at $T/T_m \leq 0.8$ was calculated to be $\bar{\rho} = 0.180$ with an error of 3.3%. Although the dependence of roughness on temperature for $T/T_m \leq 0.8$ was very small, it was not negligible: as the temperature was increased, the system experienced a thermal expansion, which was achieved by the repositioning of the atoms. Due to the PBCs along the lateral directions and the supporting atomic layer at the bottom of the system, which was fixed along the z-axis, the thermal expansion was restricted to only move the free rough surface. The surface atoms with higher potential energy values were the most favorable for changing their positions. As a consequence of the thermal expansion and repositioning process, the roughness could slightly change, and, also, more atoms could be identified as surface atoms; therefore, more data points would be accessible for fitting the surface. Figure 16 illustrates the identified surface atoms of the system along the path $0 \leq x \leq L$ at $y = 0.5L$. This figure shows how the thermal expansion affected the spatial coordinates of the surface atoms: for the selected path, the change in the temperature from 0 K to $0.6T_m$ resulted in the identification of 54 and 71 surface atoms, respectively. The higher number of identified surface atoms is related to thermally invoked atomic steps on the free

surface, which result in a higher roughness; see Appendix D for a detailed discussion on this behavior.
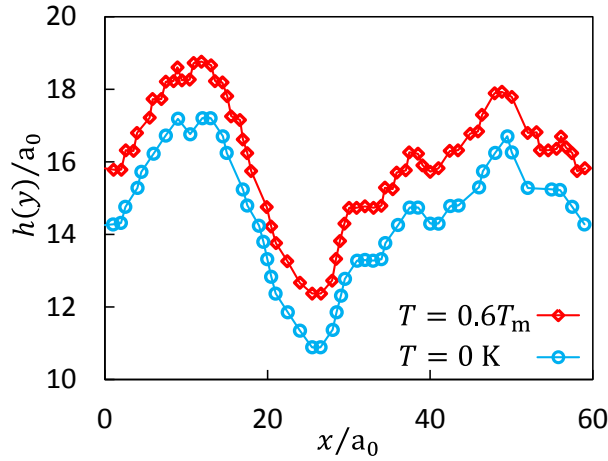
Figure 16. The identified surface atoms of the system along the path $0 \leq x \leq L$ at $y = 0.5L$ at two temperatures of 0 K and $0.6T_{\mathrm{m}}$.

All of the identified surface atoms were used for fitting a surface as described in section 4.3. The results were reported as $LR = 1a_0$ for the case that all of the data points of the fitted surface were analyzed at once; this holds for all of the reported results of this work, with the exception of Figure 15 (a), where the results for $LR = 5a_0$ were reported for comparison. For the case of $LR = 5a_0$, the first noticeable result was a lower average roughness compared to the case of $LR = 1a_0$: the average roughness was obtained to be $\bar{\rho}(LR = 5a_0) = 0.113$ compared to $\bar{\rho}(LR = 1a_0) = 0.180$ at $T/T_{\mathrm{m}} \leq 0.8$. Furthermore, the larger sampling lateral resolution made it possible to analyze the surface more than once, and the results were reported with the corresponding measurement errors. Figure 15 (a) shows that the calculated roughness values for $LR = 5a_0$ at $T/T_{\mathrm{m}} \leq 0.8$ were more or less in the same range regardless of temperature without any meaningful difference. In another words, an LR of $5a_0$ is large enough to cover any meaningful changes of roughness at a temperature range of $T/T_{\mathrm{m}} \leq 0.8$. On the other hand, the changes of roughness would be clearer by studying the q_{dev} values, as shown in Figure 15 (b); the deviating wavenumber is temperature-independent for $T/T_{\mathrm{m}} \leq 0.4$. At higher temperatures, the value of q_{dev} decreases. At the melting point, q_{dev} reaches the value of q_{L}, indicating that the surface of the molten substrate has lost its original roughness features all over the surface.

Figure 17 shows the atomic structure of the substrates at $T/T_{\mathrm{m}} = 0$ and $T/T_{\mathrm{m}} = 1$; this figure confirms that the very low value of $\rho \cong 0.05$ indicates that the surface is nearly flat. Although the roughness parameter ρ is close to its theoretical minimum of zero (see section 5.2), it does not reach this value at the melting point due to the presence of thermally excited capillary waves. Instead, the roughness

20

parameter is calculated to be $\rho \cong 0.07$ at the melting point for the simulated systems, as discussed in detail in Appendix D.
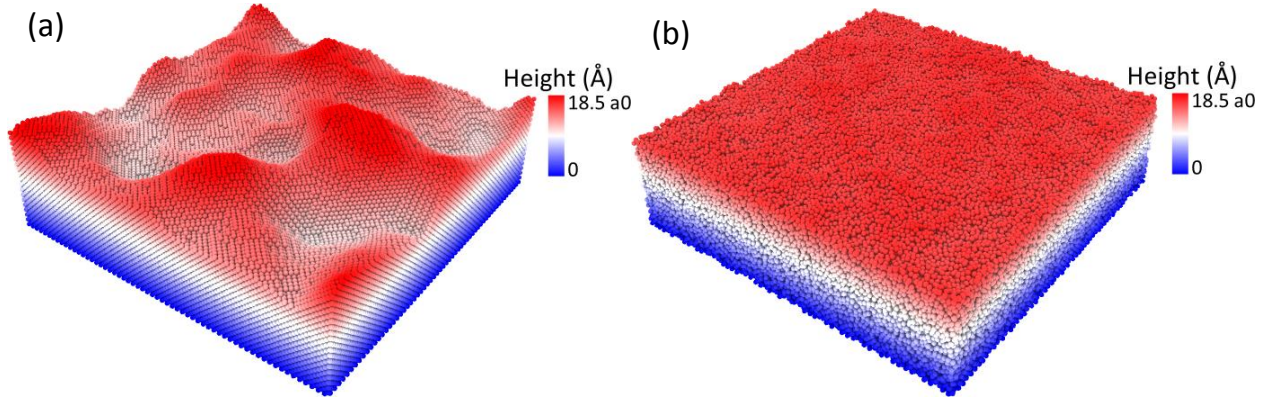
Figure 17. The atomic structure of the equilibrated substrate at (a) $T/T_{\mathrm{m}} = 0$ and (b) $T/T_{\mathrm{m}} = 1$. The atoms are colored based on their height values.

Studying the effects of temperature shows that the deviating wavenumber is temperature-independent for $\mathrm{T} \leq 0.4 T_{\mathrm{m}}$.

5.6. Generating pseudo-stable systems

In order to generate a pseudo-stable rough substrate, two different methods can be proposed based on the results of the investigated systems: one would be to set the cutoff wavenumber of the PSD to some value smaller than or equal to the minimum of the deviating wavenumbers, i.e. $q_{\mathrm{S}} \leq \min(q_{\mathrm{dev}}) \cong 0.2\,\text{Å}^{-1}$. This value translates into a wavelength of $\lambda \cong 8a_0$ and, although not being related to any critical length in an fcc structure, it can be compared with the current lateral resolution of atomic-force microscopy (AFM) utilizing carbon nanotube tips, which could be as low as $\sim 2\,\text{nm}$ [38]. For an fcc structure, however, the lateral resolution is relevant down to the interatomic spacing, where the PSD cutoff wavenumber needs to be defined by means of the shortest possible wavelength. Therefore, another method needs to be applied for resolving the deviation issue: the PSD can be described via expanding Eq. 2 into a three-segment PSD:

$$C(\mathbf{q}) = \begin{cases} C_0 & q_{\mathrm{L}} \leq \|\mathbf{q}\| < q_{\mathrm{r}} \\ C_0(\|\mathbf{q}\|/q_{\mathrm{r}})^{\beta_1} & q_{\mathrm{r}} \leq \|\mathbf{q}\| \leq q_{\mathrm{dev}} \\ C_1(\|\mathbf{q}\|/q_{\mathrm{dev}})^{\beta_2} & q_{\mathrm{dev}} \leq \|\mathbf{q}\| \leq q_{\mathrm{S}} \\ 0 & \mathrm{elsewhere} \end{cases},$$

Eq. 4

with

$$C_1 = C_0(q_{\mathrm{dev}}/q_{\mathrm{r}})^{\beta_1}.$$

Eq. 5

Following the discussion in Appendix B and using Eq. B1, in order to generate a rough surface tuned to an assigned value of σ_{rms}, the value of C_0 needs to be calculated from

$$C_0 = \frac{\sigma_{\mathrm{rms}}^2}{2\pi}V^{-1},$$

Eq. 6

with

$$V = \frac{q_{\mathrm{r}}^2 - q_{\mathrm{L}}^2}{2} + q_{\mathrm{r}}^{-\beta_1}\left(\frac{q_{\mathrm{dev}}^{2+\beta_1} - q_{\mathrm{r}}^{2+\beta_1}}{2+\beta_1} + q_{\mathrm{dev}}^{\beta_1-\beta_2}\frac{q_{\mathrm{S}}^{2+\beta_2} - q_{\mathrm{dev}}^{2+\beta_2}}{2+\beta_2}\right).$$

Eq. 7

In order to examine the applicability of the proposed methods, three different surfaces were generated: one surface using Eq. 2 with $q_{\mathrm{S}} \cong 0.2\ \text{Å}^{-1}$, and one using Eq. 3 with $q_{\mathrm{S}} \cong 0.2\ \text{Å}^{-1}$ and $\zeta = 5a_0$; the PSD exponent for these two surfaces was selected to be $\beta = -3.5$. The third surface was generated using Eq. 4 with $q_{\mathrm{dev}} \cong 0.2\ \text{Å}^{-1}$, $q_{\mathrm{S}} = 2\pi/\lambda_{\mathrm{min}}$, $\beta_1 = -3.5$, and $\beta_2 = -4.5$. The RMS roughness for all of surfaces was selected to be $\sigma_{\mathrm{rms}} = 2a_0$. The generated surfaces were used for building corresponding substrates as described in section 4.1, and the substrates were relaxed at zero Kelvin via the conjugate gradient algorithm [34], as described in section 4.2. The reason for relaxing the systems at zero Kelvin is based on the findings of section 5.5: the changes of the surface roughness are temperature-independent for $T \leq 0.4T_{\mathrm{m}}$.

Figure 18 shows the PSDs of the rough surfaces before and after the equilibration process: the results

show no difference between the original and the equilibrated PSDs. In other words, both of the proposed

methods can be used to generate pseudo-stable rough substrates.

Furthermore, the applicability of the proposed methods was studied via another set of three surfaces, where all parameters were the same as the previous ones, but their RMS roughness was set to a larger value of $\sigma_{rms} = 5a_0$. The PSDs of the rough surfaces are shown in Figure 19: while there is no difference between the original and the equilibrated PSDs for wavenumbers smaller than $0.2\,\text{Å}^{-1}$, the deviations can be detected for larger wavenumbers.
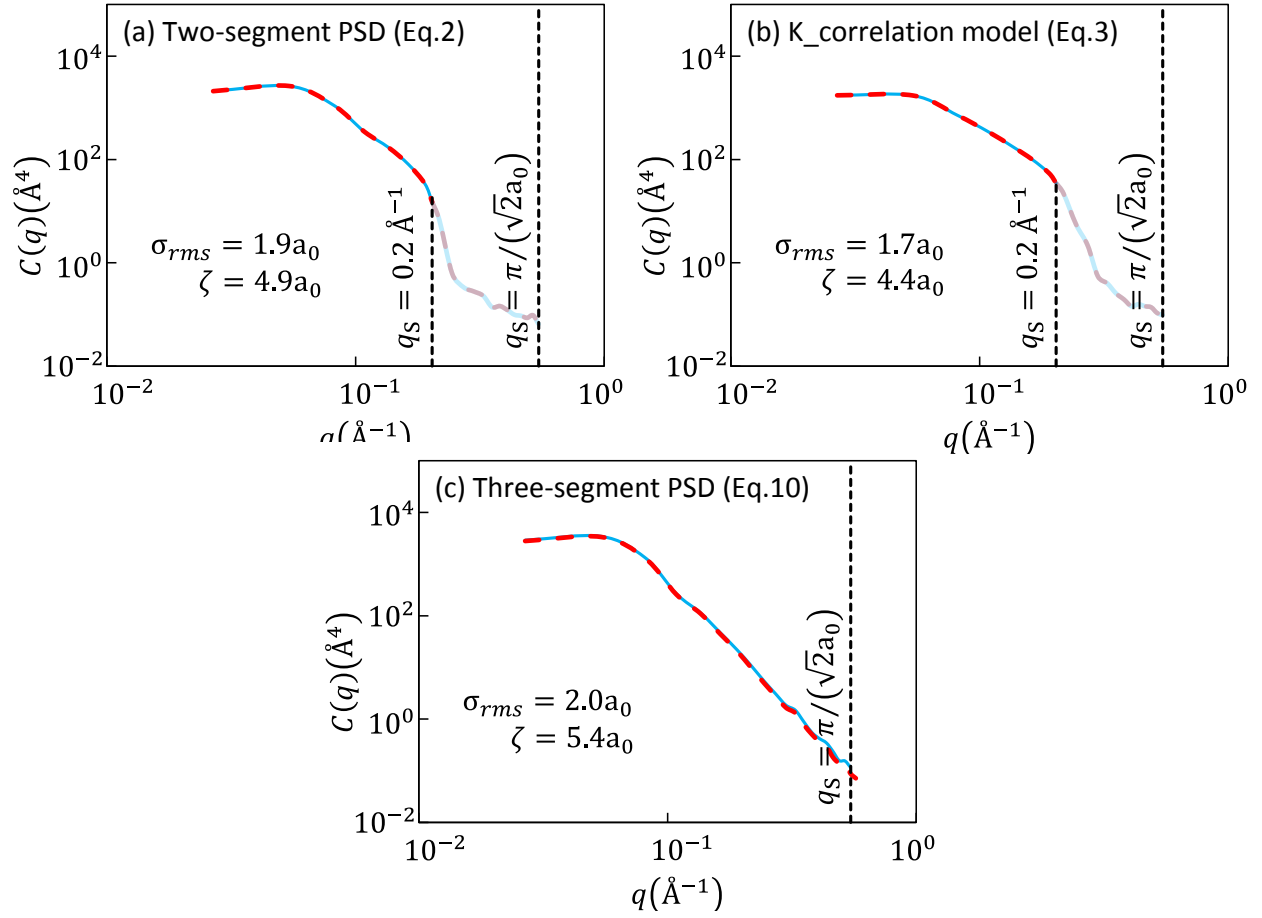
Figure 18. The PSDs of the surface roughness of the generated (continuous line) and equilibrated substrates (dashed line). The surfaces were generated using (a) the two-segment PSD Eq. 2, (b) the K-correlation model Eq. 3, and (c) the extended PSD model in the form of Eq. 4. It should be noted that the PSDs used for generating surfaces in (a) and (b) had a cutoff of $q_S = 0.2$ Å^{-1}; however, for analyzing the surfaces, a natural cutoff of $q_S = 2\pi/\lambda_{min}$ was used. That is why the plots are shown with a different shading between the assigned cutoff and the natural one.
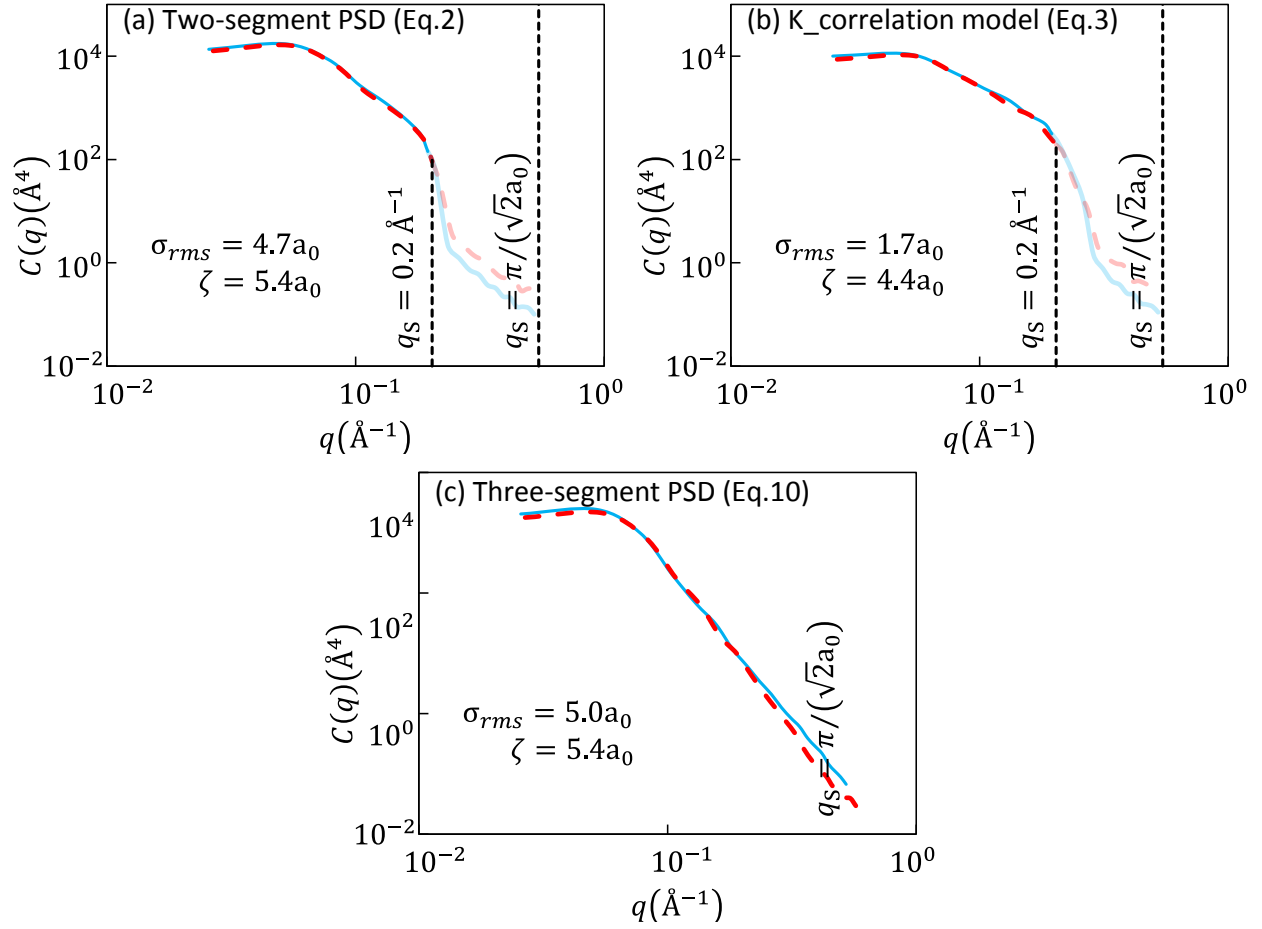
Figure 19. The PSDs of the surface roughness of the generated (continuous line) and equilibrated substrates (dashed line). The surfaces were generated using (a) the two-segment PSD Eq. 2, (b) the K-correlation model Eq. 3, and (c) the extended PSD model in the form of Eq. 4. For the explanation of different values of q_S on (a) and (b), the readers are referred to the caption of Figure 18.

6. Conclusions

The results of this investigation show that rough surface topography needs to be defined in a physically meaningful manner for implementation in atomistic simulations. Thermodynamically, rough surfaces under equilibration tend to have their atomic steps and edges removed in order to lower the potential energy of the system, and reach the local minimum of energy; as a result, the equilibration procedure smoothens the rough surfaces as the changes of skewness and kurtosis of the equilibrated surfaces under investigation in this work confirm.

In this paper, different quasi-fractal rough surfaces were generated, which were used for constructing rough atomistic blocks of gold with different crystal orientations. Then, the blocks were relaxed and

equilibrated at different temperatures. The surface roughness of the equilibrated substrates was analyzed and compared with the corresponding original rough surface. In order to study the surface roughness, a hybrid roughness parameter was defined as $\rho = \sigma_{rms}\overline{g}/\zeta$, which has a value of $\rho = 0$ for a perfectly flat surface, and increases as the surface becomes randomly rougher.

It was found that rougher surfaces experience larger roughness changes, and the dependence of these changes on crystal orientation is negligible. Moreover, the changes in the surface roughness were found to be temperature-independent for $T/T_m \leq 0.4$.

Furthermore, the rough surfaces were analyzed through their PSDs. It was found that the substrates could hold their original PSDs up to a wavenumber denotes q_{dev}, where the deviation occurred for larger wavenumbers. A minimum value of $0.2\,\text{Å}^{-1}$ was found for this deviating wavenumber, i.e. $q_{dev} \geq 0.2\,\text{Å}^{-1}$. This finding was used for proposing two different methods to generate pseudo-stable rough substrates: one is to set the high frequency cutoff to the obtained minimum value for the q_{dev}, i.e. $q_S = 0.2\,\text{Å}^{-1}$. This situation can be amenable to comparisons with measurements performed with an AFM utilizing carbon nanotube tips featuring a high lateral resolution of $\sim$2 nm [38]. This method was tested for different systems, where the results showed no differences in their PSD before and after the relaxation process. The other method for generating rough surfaces was obtained by defining a three-segment PSD, described in Eq. 4. The method was tested for two different RMS roughness values of $2a_0$ and $5a_0$. Analyzing the PSDs showed that, for the substrate with $\sigma_{rms} = 2a_0$, there were no changes in the surface roughness due to the relaxation process; however, the substrate with $\sigma_{rms} = 5a_0$ showed deviations at high wavenumbers larger than $q_{dev} = 0.2\,\text{Å}^{-1}$. The detected deviations in the final simulations (see Figure 19) for wavelengths larger than $q_S = 0.2\,\text{Å}^{-1}$, indicate that, if the lateral resolution needs to be finer than $2\sim3$ nm, the system has to be relaxed regardless of its initial roughness, otherwise the rough surface representation would be non-physical.

The results of the current investigation reveal that, rough surfaces used in atomistic simulations need to be properly equilibrated, regardless of their initial roughness, unless the lateral resolutions finer than $\sim$8a_0 are not of interest. . It should be noted that this statement would be valid only for the roughness of free surfaces, i.e. before the occurrence of any type of contact; the changes of the surface roughness due to contact are not the focus of this research and have been studied extensively [3, 7-12].

Moreover, for the relaxation process, the initial block does not need to be thick, because dislocation emissions, if any, would be extremely limited during equilibration. Moreover, if the simulation

temperature is lower than $0.4T_\mathrm{m}$, instead of molecular dynamics, molecular statics (resembling 0 K) can be employed to relax the rough substrate.

Appendix A

For self-affine fractal profiles, the PSD exponent would be [39]

$$\beta = -(2H + D_T),$$

<div align="right">Eq. A1</div>

where H is the Hurst exponent, and D_S is the spatial dimension of the projected fractal, i.e. $D_S = 2$ for a fractal surface and $D_S = 1$ for a fractal line. The Hurst exponent describes the raggedness of the profile, with a lower value leading to a rougher profile. The value of the Hurst exponent is bounded as $0 < H < 1$. Considering the range of the Hurst exponent, one may conclude that $\beta \in (-2, -4)$ for a fractal surface. The definition of the PSD in the form of Eq. 2, however, does not apply such a restriction on the values of β. On the other hand, if β exceeds the abovementioned limitation, the value of H would vary outside the range of $(0,1)$; therefore, H loses its general meaning of the Hurst exponent [40]. This is the main reason why the PSD exponent is not expressed in terms of H or D_F in the current study.

Appendix B

The spectral moments of the PSD can be calculated from [41]

$$m_n = A_n \int_0^{+\infty} q^{1+n} C(q)\,\mathrm{d}q,$$

<div align="right">Eq. B1</div>

with

$$A_n = \int_0^{2\pi} (\cos \omega)^n \, d\omega.$$

<div align="right">Eq. B2</div>

For $n = 0, 2$, and 4, A_n equals 2π, π, and $3\pi/4$, respectively. Considering the definition of $C(q)$ for $q_\mathrm{L} \leq q \leq q_\mathrm{S}$ based on Eq. 2, Eq. B1 can be solved and reformulated as follows:

$$m_n = A_n C_0 q_r^{2+n} I_n,$$

<div align="right">Eq. B3</div>

with

$$I_n = \frac{1 - M_L^{2+n}}{2+n} - \frac{1 - M_S^{2+n+\beta}}{2+n+\beta},$$

<div align="right">Eq. B4</div>

where $M_L = q_L/q_r$, and $M_S = q_S/q_r$. These formulae are important for the generation of rough surfaces; a rough surface can be generated by solving Eq. 1, where the values of $h(\mathbf{q})$ should be converted from the values of $C(\mathbf{q})$ in the form of Eq. 2. In order to solve Eq. 2, the values of q_L, q_r, q_S, β, and C_0 need to be defined beforehand. The values of these variables can be assigned arbitrarily, provided they do not violate the conditions of $q_L < q_r < q_S$, $\beta < 0$, and $C_0 > 0$. The value of C_0, however, can be defined such that the generated surface will possess a specific spectral moment. Considering that $m_0 = \sigma_{rms}^2$ [16], and $m_2 = \frac{1}{2}\overline{g}^2$ [42], the parameter C_0 can be defined as $C_0 = \sigma_{rms}^2 (A_0 I_0 q_r^2)^{-1}$ and $C_0 = \frac{1}{2}\overline{g}^2 (A_2 I_2 q_r^4)^{-1}$, respectively. In order to generate a surface with given values of σ_{rms} and $\overline{g}$, however, C_0 will need to have a unique solution, resulting in a distinctive roll-off wavenumber of $q_r = (\overline{g}/\sigma_{rms})\sqrt{I_0/I_2}$, which cannot be solved analytically. Therefore, in this study, C_0 was estimated based on the PSD's zeroth moment, in order to generate rough surfaces with a specific value of σ_{rms}.

Appendix C

For an atomistic nominally flat rough surface, a limiting case would be a saw-tooth rough surface, with every other atom removed along each of the lateral directions. In the surface analysis methods adapted in this work, the atomistic rough surfaces were projected on a uniformly gridded plane. The estimated surface for the abovementioned limiting case is shown in Figure C1. It can be shown that the local gradient on each grid point is $\sqrt{2}$. Consequently, the mean gradient of this limiting case would be $\sqrt{2}$.
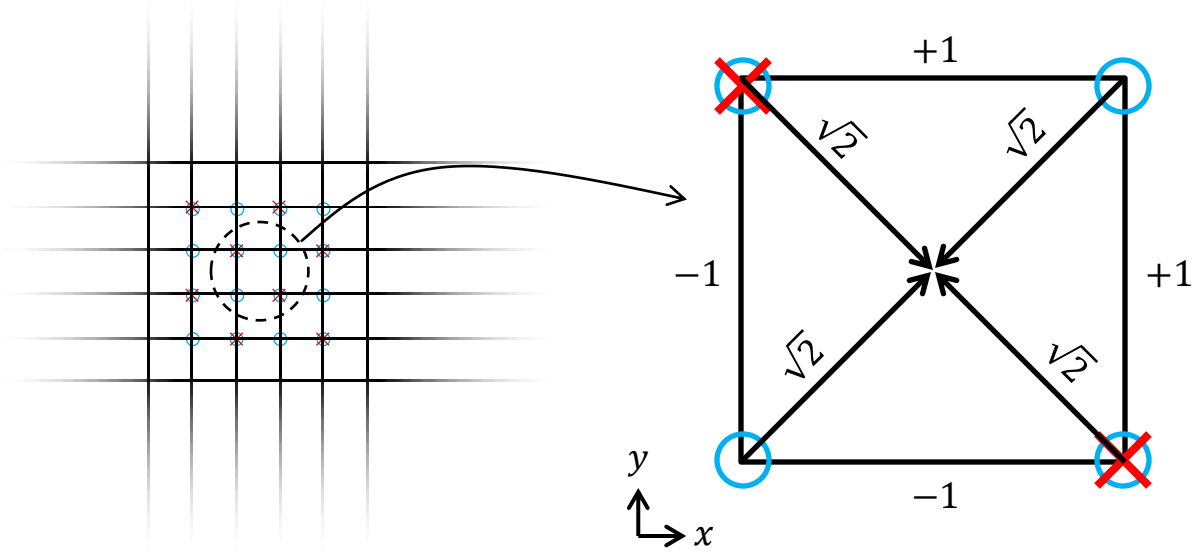
Figure C1. (Left) The uniformly gridded plane for the limiting case of an atomistic nominally flat rough surface along the $\{001\}$ planes of an fcc structure, where every other atom is removed along each direction of x and y. Note that no grid was assigned for the faced-centered atoms in the surface analysis of the current work. (Right) A selected grid of the saw-tooth rough surface. The numbers on the edges indicate the calculated slopes along the x and y axes. The numbers on the arrows indicate the local gradients at each grid point.

Appendix D

The interface undulation between any two fluids can be described by capillary wave theory; see [43] for a short review, and [44] for a deep discussion on the applicability of this theory in MD simulations. While this theory is most relevant for interfaces between fluids, one may argue that it is still applicable for the cases studied in this research, i.e. the free surface of a solid, specifically for studying the effect of temperature on the surface roughness.

In capillary wave theory, the thermally excited height fluctuation spectrum $h_{\mathrm{CW}}(q)$ of an isotropic crystallographic surface can be expressed by:

$$\langle |h_{\mathrm{CW}}(q)|^2 \rangle = \frac{k_B T}{\gamma L^2} q^{-2}, \qquad \text{Eq. D1}$$

where k_B is the Boltzmann constant, and γ is the surface energy of the free surface expressed in the dimensions of energy over area. Considering the relation $C(q) = (L/2\pi)^2 \langle |h(q)|^2 \rangle$ (see section 2), the

power spectral distribution of the thermally agitated capillary waves can be written as

$$C_{CW}(q) = \frac{1}{4\pi^2} \frac{k_B T}{\gamma} q^{-2}. \qquad \text{Eq. D2}$$

The RMS roughness of the thermally agitated capillary waves can be obtained from m_0 (see Appendix B) to be

$$\sigma_{\text{rms,CW}} = \left(\frac{1}{2\pi} \frac{k_B T}{\gamma} \ln\left(\frac{L}{\delta}\right) \right)^{0.5}. \qquad \text{Eq. D3}$$

Therefore, the total RMS roughness of the surface can be estimated as

$$\sigma_{\text{rms}} = \sqrt{\sigma_{\text{rms,0}}^2 + \sigma_{\text{rms,CW}}^2}. \qquad \text{Eq. D4}$$

Considering Eq. D3 and the proportionality of $C_{CW} \propto T$, one may argue that the roughness would be higher as the equilibration temperature increases. This would be in accord with the reported results in section 5.5.

As the temperature rises, the material softens and cannot withstand the local stresses due to the initial surface roughness, as is particularly visible for the case of $T = T_m$; however, the generated capillary waves do not allow the surface to have a roughness parameter of $\rho = 0$. In order to estimate the roughness parameter of the free surface at the melting point, one can assume that the surface roughness is solely due to capillary waves. Therefore, the RMS roughness can be calculated via Eq. D3. Moreover, the mean gradient can be calculated from m_2 (see Appendix B) to be

$$\overline{g}_{CW} = \left(\pi \frac{k_B T}{\gamma} (\delta^{-2} - L^{-2}) \right)^{0.5}. \qquad \text{Eq. D5}$$

Furthermore, the autocovariance function of the power spectral distribution in the form of Eq. D2 can be calculated using the zero-order Hankel transform of $C(q)$, which results in

$$\text{var}(r) = \frac{1}{2\pi} \int_{q_L}^{q_S} C(q) J_0(qr) q dq \,,$$
<div align="right">Eq. D6</div>

where J_0 is the zero-order Bessel function of the first kind. Then, the autocorrelation function can be calculated as $R(r) = \text{var}(r)/\text{var}(\delta)$.

For the simulated material, the melting point and the (100) surface energy are 1281 K and $1.225\,\text{J/m}^2$, respectively [28]. Inserting these values into Eq. D3, Eq. D5, and Eq. D6, yields values for the RMS roughness, mean gradient, and lateral correlation length of $\sigma_{\text{rms,CW}} = 0.6a_0$, $\overline{g}_{\text{CW}} = 0.5$, and $\zeta_{\text{CW}} = 4.7a_0$, respectively. It should be noted that the lateral correlation length was estimated from the numerical solution of Eq. D6 (see Figure D1). Thus, the roughness parameter of the molten system can be calculated as $\rho_{\text{CW}} \cong 0.07$, which is very close to the measured value of $\rho \cong 0.05$ for the system at the melting point (see section 5.5).
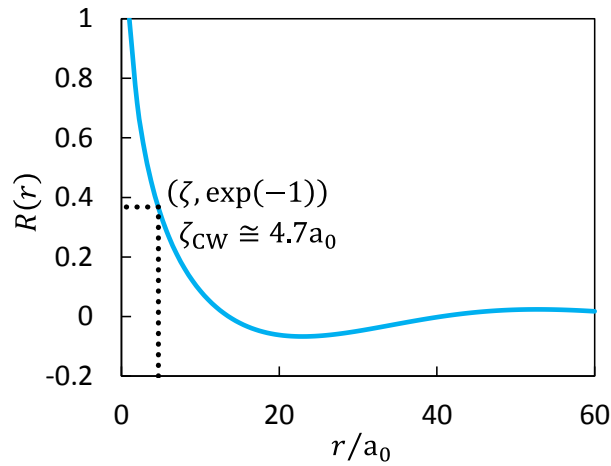

Figure D1. The autocorrelation function of the thermally agitated capillary waves on a free surface of a gold substrate at the melting point.

References

[1] J.P. Ewen, S. Echeverri Restrepo, N. Morgan, D. Dini, Nonequilibrium molecular dynamics simulations of stearic acid adsorbed on iron surfaces with nanoscale roughness, Tribology International, 107 (2017) 264-273.

[2] S. Solhjoo, A.I. Vakis, Continuum mechanics at the atomic scale: Insights into non-adhesive contacts using molecular dynamics simulations, Journal of Applied Physics, 120 (2016) 215102.

[3] S. Solhjoo, A.I. Vakis, Normal Contacts of Lubricated Fractal Rough Surfaces at the Atomic Scale, in: TriboUK 2015, Loughborough, 16-17 April 2015, p. 36.

[4] S. Solhjoo, A.I. Vakis, Lubricated normal and sliding contact of fractal rough surfaces at the atomic scale, in: The International Conference on Understanding and Controlling Nano and Mesoscale Friction, Istanbul, 22-26 June 2015, p. 46.

[5] S.J. Eder, G. Feldbauer, D. Bianchi, U. Cihak-Bayr, G. Betz, A. Vernes, Applicability of Macroscopic Wear and Friction Laws on the Atomic Length Scale, Physical Review Letters, 115 (2015).

[6] H.T. Zhu, X. Zheng, P.B. Kosasih, A.K. Tieu, Tribo-surface charge and polar lubricant molecules on friction and lubrication under multiple 3D asperity contacts, Wear, 332 (2015) 1248-1255.

[7] S. Solhjoo, A.I. Vakis, Molecular dynamics simulations of rough contact with fractal and statistical surface generation, in: ASME 2014 12th Biennial Conference on Engineering Systems Design and Analysis, American Society of Mechanical Engineers, 2014, pp. V003T014A002.

[8] X. Zheng, H. Zhu, A.K. Tieu, B. Kosasih, Roughness and Lubricant Effect on 3D Atomic Asperity Contact, Tribology Letters, 53 (2014) 215-223.

[9] X. Zheng, H. Zhu, A. Kiet Tieu, B. Kosasih, A molecular dynamics simulation of 3D rough lubricated contact, Tribology International, 67 (2013) 217-221.

[10] P. Spijker, G. Anciaux, J.-F. Molinari, Relations between roughness, temperature and dry sliding friction at the atomic scale, Tribology International, 59 (2013) 222-229.

[11] P. Spijker, G. Anciaux, J.-F.o. Molinari, The effect of loading on surface roughness at the atomistic level, Computational Mechanics, 50 (2012) 273-283.

[12] P. Spijker, G. Anciaux, J.-F. Molinari, Dry Sliding Contact Between Rough Surfaces at the Atomistic Scale, Tribology Letters, 44 (2011) 279-285.

[13] D.J. Oliver, W. Paul, M.E. Ouali, T. Hagedorn, Y. Miyahara, Y. Qi, P.H. Grütter, One-to-one spatially matched experiment and atomistic simulations of nanometre-scale indentation, Nanotechnology, 25 (2014) 025701.

[14] S. Solhjoo, A.I. Vakis, Single asperity nanocontacts: comparison between molecular dynamics simulations and continuum mechanics models, Computational Materials Science, 99 (2015) 209-220.

[15] S. Solhjoo, A.I. Vakis, Definition and detection of contact in atomistic simulations, Computational Materials Science, 109 (2015) 172-182.

[16] P.R. Nayak, Random Process Model of Rough Surfaces, Journal of Lubrication Technology, 93 (1971) 398-407.

[17] B.N.J. Persson, O. Albohr, U. Tartaglino, A.I. Volokitin, E. Tosatti, On the nature of surface roughness with application to contact mechanics, sealing, rubber friction and adhesion, Journal of Physics-Condensed Matter, 17 (2005) R1-R62.

[18] B. Bhushan, A. Majumdar, ELASTIC PLASTIC CONTACT MODEL FOR BIFRACTAL SURFACES, Wear, 153 (1992) 53-64.

[19] J.J. Wu, Characterization of fractal surfaces, Wear, 239 (2000) 36-47.

[20] C. Borri, M. Paggi, Topology simulation and contact mechanics of bifractal rough surfaces*, Proceedings of the Institution of Mechanical Engineers Part J-Journal of Engineering Tribology, 230 (2016) 1345-1358.

[21] J. Bae, I.J. Lee, A bifractal nature of reticular patterns induced by oxygen plasma on polymer films, Scientific Reports, 5 (2015).

[22] G. Palasantzas, ROUGHNESS SPECTRUM AND SURFACE WIDTH OF SELF-AFFINE FRACTAL SURFACES VIA THE K-CORRELATION MODEL, Physical Review B, 48 (1993) 14472-14478.

[23] M. Pelliccione, T.-M. Lu, Evolution of Thin-Film Morphology, Springer, 2008.

[24] B. Luan, M.O. Robbins, Contact of single asperities with varying adhesion: Comparing continuum mechanics to atomistic simulations, Physical Review E, 74 (2006) 026111.

[25] M.P. Allen, D.J. Tildesley, Computer Simulation of Liquids, Clarendon Press, 1989.

[26] J.M. Haile, Molecular Dynamics Simulation: Elementary Methods, Wiley, 1992.

[27] A.P. Rigazzi, The effects of roughness on the area of contact and on the elastostatic friction, in, Università della Svizzera Italiana, 2014.

[28] H.W. Sheng, M.J. Kramer, A. Cadien, T. Fujita, M.W. Chen, Highly optimized embedded-atom-method potentials for fourteen fcc metals, Phys.Rev.B, 83 (2011) 134118.

[29] S. Plimpton, Fast parallel algorithms for short-range molecular dynamics, Journal of Computational Physics, 117 (1995) 1-19.

[30] W.C. Swope, H.C. Andersen, P.H. Berens, K.R. Wilson, A computer simulation method for the calculation of equilibrium constants for the formation of physical clusters of molecules: Application to small water clusters, The Journal of chemical physics, 76 (1982) 637-649.

[31] S. Solhjoo, A. Simchi, H. Aashuri, Molecular dynamics simulation of melting, solidification and remelting processes of aluminum, Iranian Journal of Science and Technology-Transactions of Mechanical Engineering, 36 (2012) 13-23.

[32] M.S. Daw, M.I. Baskes, Embedded-atom method - derivation and application to impurities, surfaces, and other defects in metals, Physical Review B, 29 (1984) 6443-6453.

[33] H.J.C. Berendsen, J.P.M. Postma, W.F. van Gunsteren, A. DiNola, J.R. Haak, Molecular dynamics with coupling to an external bath, The Journal of chemical physics, 81 (1984) 3684-3690.

[34] E. Polak, G. Ribiere, Note sur la convergence de méthodes de directions conjuguées, Revue Francaise D Informatique De Recherche Operationnelle, 3 (1969) 35-43.

[35] A. Stukowski, Visualization and analysis of atomistic simulation data with OVITO–the Open Visualization Tool, Modelling and Simulation in Materials Science and Engineering, 18 (2010) 015012.

[36] I. Amidror, Scattered data interpolation methods for electronic imaging systems: a survey, Journal of Electronic Imaging, 11 (2002) 157-176.

[37] E.S. Gadelmawla, M.M. Koura, T.M.A. Maksoud, I.M. Elewa, H.H. Soliman, Roughness parameters, Journal of Materials Processing Technology, 123 (2002) 133-145.

[38] C.V. Nguyen, K.J. Chao, R.M.D. Stevens, L. Delzeit, A. Cassell, J. Han, M. Meyyappan, Carbon nanotube tip probes: stability and lateral resolution in scanning probe microscopy and application to surface science in semiconductors, Nanotechnology, 12 (2001) 363-367.

[39] G. Dougherty, Appendix C, in: Digital Image Processing for Medical Applications, Cambridge University Press, 2009, pp. 423-431.

[40] R. Pohrt, V. Popov, M. Heß, Normal Contact of Rough Surfaces, in: Method of Dimensionality Reduction in Contact Mechanics and Friction, Springer Berlin Heidelberg, 2014, pp. 143-164.

[41] B. Lorenz, Contact Mechanics and Friction of Elastic Solids on Hard and Rough Substrates in, Forschungszentrums Jülich, Jülich, Germany, 2012.

[42] W. Manners, J.A. Greenwood, Some observations on Persson's diffusion theory of elastic contact, Wear, 261 (2006) 600-610.

[43] D. Aarts, M. Schmidt, H.N.W. Lekkerkerker, Direct visual observation of thermal capillary waves, Science, 304 (2004) 847-850.

[44] J.J. Hoyt, Z.T. Trautt, M. Upmanyu, Fluctuations in molecular dynamics simulations, Mathematics and Computers in Simulation, 80 (2010) 1382-1392.